American Mineralogist, Volume 93, pages 1874–1881, 2008

Structural transition of post-spinel phases $CaMn_2O_4$, $CaFe_2O_4$, and $CaTi_2O_4$ under high pressures up to 80 GPa

T. YAMANAKA,[1,2,*] A. UCHIDA,[1] AND Y. NAKAMOTO[2]

[1]Earth and Space Science, Graduate School of Science, Osaka University, 1-1 Machikaneyama, Toyonaka 560-0043, Osaka, Japan
[2]Research Center for Quantum Science and Technology Under Extreme Conditions, Osaka University, Japan

ABSTRACT

Three structures of $CaMn_2O_4$, $CaFe_2O_4$, and $CaTi_2O_4$ have been proposed as post-spinel phases. Because these structures are very similar, several ambiguities and inconsistencies appear in high-pressure studies, leading to many problems that are yet to be solved. Systematic powder diffraction studies related to these three phases were conducted under high pressure using synchrotron radiation. All three samples have further high-pressure polymorphs. $CaMn_2O_4$ transforms to the $CaTi_2O_4$-type structure at about 30 GPa. The MnO_6 octahedron in the lower-pressure structure is distorted by the Jahn-Teller effect. A new phase was observed at pressures above 50 GPa during compression of $CaFe_2O_4$. Rietveld profile fitting analysis of diffraction data at 63.3 GPa demonstrated that the high-pressure structure, with space group *Pnam*, is produced via a martensitic transformation by displacing atoms in every third layer perpendicular to the *c* axis. $CaTi_2O_4$ also has a new high-pressure polymorph above 39 GPa with space group *Bbmm*. The most probable post-spinel candidate in the mantle is the $CaTi_2O_4$-type structure. The $CaMn_2O_4$-type structure is only formed at high pressure from spinel phases with atoms susceptible to Jahn-Teller distortion.

Keywords: Post-spinel, high-pressure diffraction, structure transition, $CaMn_2O_4$, $CaFe_2O_4$, $CaTi_2O_4$

INTRODUCTION

Much attention has been paid to high-pressure structural transitions of the many spinel phases in the crust of the Earth due to their geophysical importance (Reid and Ringwood 1969; Ito et al. 1989; Irifune et al. 1998). One of the major minerals in the crust, Mg_2SiO_4 olivine, transforms to wadsleyite (β-spinel) and further to ringwoodite (γ-phase) with the spinel structure (Meng et al. 1993; Morishima et al. 1994). These high-pressure transformations are significant subjects for seismic interpretation (Leven et al. 1981; Burnley et al. 1991; Shim et al. 2001). Oxide spinels with transition elements or mixed-charge cations have been intensively studied from various viewpoints such as their magnetic, electronic, or elastic properties (Sawamoto et al. 1984; Kiefer et al. 1997; Li et al. 2007). Various spinel structures (Hill et al. 1979; Lavina et al. 2002) result from the different cation distributions in the A (tetrahedral) and B (octahedral) sites. Many spinels have been reported to have solid solutions between cations in the A and B sites. Intra-crystalline cation exchange in these sites has also been reported from high-temperature studies, such as an order-disorder transition in $MgAl_2O_4$ (Yamanaka et al. 1983; Peterson et al. 1991; Pavese et al. 1999; Harrison et al. 1999; Méducin et al. 2004). Silicate spinels of transition elements are significant samples for magnetic and electric conduction in the crust and mantle and their phase stabilities and structures under high-pressure and high-temperature conditions have been intensively studied (Ohtaka et al. 1997; Xu et al. 1998; Yamanaka and Okita 2001; Yamanaka et al. 2001). High-pressure structure transitions of various AB_2O_4 spinels in the crust have also been given increased attention to understand their structures in the lower mantle or subduction zones (Irifune et al. 1991; Kirby et al. 1996). Their structure transitions or decompositions under high pressures are summarized in Figure 1.

As shown in the list of high-pressure structures of spinels (Table 1), Raman spectroscopy and powder diffraction studies have resulted in three proposed orthorhombic phases of $CaMn_2O_4$-, $CaTi_2O_4$-, and $CaFe_2O_4$-type structures as high-pressure polymorphs of spinels. In these three structures, Ca atoms are located at an eightfold-coordinated site and Mn, Ti, and Fe atoms are on a sixfold-coordinated site. The octahedra are linked through both shared edges and corners. Therefore, these three structure types have much denser structures than their spinel counterparts.

The simulated powder diffraction patterns, based on single-crystal analyses of $CaMn_2O_4$ (Geisber et al. 2001), $CaTi_2O_4$ (Rogge et al. 1998), and $CaFe_2O_4$ (Decker et al. 1957) are nearly identical, highlighting the similarity in the three structures. Their space groups, lattice parameters, and site symmetries are presented together with their structures in Figure 2. The second lattice setting with $b > a > c$ is applied in the list for structural consistency. The three structures are composed of a herringbone octahedra array.

Powder-diffraction studies of these samples require special care because of their structural similarity. Phase identification under high pressures has proven to be very difficult because of the many overlapping peaks and the very poor resolution that occurs after the transition from spinel, which results in broadened reflection peaks. Therefore, the need remains for higher resolution high-pressure studies that are able to resolve several

* Present address: Carnegie Institute of Washington, Geophysical Laboratory, 5251 Broad Branch Road NW, Washington, D.C. 20015. E-mail: t.yamanaka@kce.biglobe.ne.jp

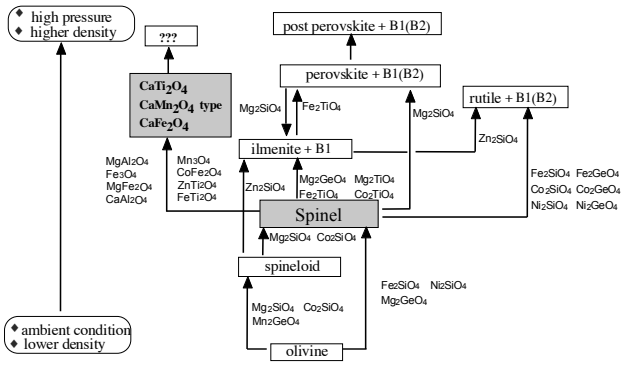

FIGURE 1. Diagram of the structure transitions and decompositions of spinels. B1 structure is a face-centered cubic structure such as NaCl and B2 a body-centered cubic structure such as CsCl.

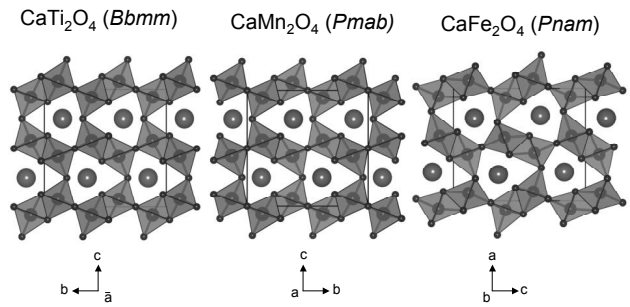

FIGURE 2. Structure comparison of the three post-spinel phases. All orthorhombic structures have the second lattice setting. Ti, Mn, and Fe atoms are in sixfold coordination, and Ca is in eightfold coordination.

problems and the confusion in the literature. The present study aims to clarify these structure relationships and to characterize the further transitions of the post-spinels.

EXPERIMENTAL METHODS

Powder samples of $CaMn_2O_4$ and $CaFe_2O_4$ were prepared by solid-solid reaction at 1250 °C at ambient pressure. The reagent grade $CaCO_3$, Fe_2O_3, and MnO_2 were mixed for the stoichiometric compositions of these samples. The mixture was first calcined in a platinum crucible. Then the quenched samples were pulverized and again heated for 20 h. These procedures were repeated three times to synthesize a homogeneous sample. $CaTi_2O_4$ synthesized by an electrochemical method (Schwandt and Fray 2005) was used for the present high-pressure study. The chemical compositions of the synthesized samples were checked by electron probe microanalysis (EPMA) and their chemical homogeneity was examined in compositional images by energy-dispersive spectrometry (EDS). Neither trace element impurities nor inhomogeneity were found in the samples.

X-ray powder diffraction experiments under high pressure were performed up to 80 GPa at room temperature using a lever-type diamond anvil cell with culets 350 μm in diameter. A rhenium gasket was preindented from 200 to 50 μm. Pressure measurement was carried out by the ruby fluorescence method (Piermarini et al. 1975; Mao et al. 1986). The sample was placed in the gasket hole with a diameter of 125 μm, together with the pressure-transmitting medium of ethanol-methanol-water mixture in the experiments up to 15 GPa. Above this pressure we did not use any pressure-transmitting medium. The sample had a fine grain size, as it was taken from the floating particles in the alcohol to avoid spotty diffraction powder rings. Angle-dispersive diffraction studies were undertaken using synchrotron radiation emitted from the storage ring at Photon Factory (KEK), Tsukuba operating at 2.5 GeV and 360 mA. A flat cassette-type imaging plate detector was employed at the undulator beam line BL-13A using a monochromatic beam of about 30 keV, and at the bending magnet beam line BL-18C using about 20 keV. With a beam of 15–45 μm collimated through the focusing mirrors, the exposure time for each diffraction pattern was about 20 min. A precise profile analysis within $2\theta = 5{\sim}15°$ was also carried out using a narrow collimator of 15 μm and a long camera length measurement at BL-18C to clarify the transition pressure and to split the overlapped peaks.

LATTICE PARAMETERS AND UNIT-CELL VOLUME OF THE THREE PHASES

To keep structure consistency of the three samples and to avoid confusion, the space group of $CaMn_2O_4$ was fixed to *Pmab,* $CaFe_2O_4$ to *Pnam,* and $CaTi_2O_4$ to *Bbmm.* The space groups appear different from those in previous literature, but this is only due to the changed settings. The axial relations between the present settings and the standard space group in *International Tables for Crystallography* (Hahn 1983) are as follows:

	Standard setting	Present setting
$CaMn_2O_4$	*Pbcm* (*a b c*)	*Pmab* (*–c b a*)
$CaFe_2O_4$	*Pnma* (*a b c*)	*Pnam* (*a c b*)
$CaTi_2O_4$	*Cmcm* (*a b c*)	*Bbmm* (*b c a*)

Rietveld profile fitting has been performed with the collected powder diffraction patterns. The lattice parameters and unit-cell volumes of all three post-spinel phases and their higher-pressure phases are listed in Table 2 from the converged structural parameters. The reliability factors of the profile fittings, R_I, R_F, R_p, R_{wp}, and S, are also presented in Table 2.

Pressure dependencies of the lattice parameters of the three phases and their higher-pressure phases are plotted in Figure 3. The lattice parameters of the latter phases are compared to those of the lower-pressure phases. The changes of the unit-cell volumes with pressure are presented in Figure 4. The data of volumes are normalized to $Z = 1$ accounted for changed Z during phase transitions.

High-pressure diffraction study of $CaMn_2O_4$ (marokite)

Powder diffraction studies of $CaMn_2O_4$ were undertaken at pressures up to 75 GPa at BL-18C and 54.5 GPa at BL-13A. Selected powder patterns taken at BL-13A are presented in Figure

TABLE 1. List of post-spinel phases and their transition pressures

Sample composition	Transition pressure (GPa)	Post-spinel phase structure type	Measurements	Reference
$MgAl_2O_4$	25	$CaFe_2O_4$	XRD	Irifune et al. (1991)
$MgAl_2O_4$	40	$CaTi_2O_4$	XRD	Funamori et al. (1998)
$(Mg_{0.1}Ca_{0.9})Al_2O_4$	20–21	$CaFe_2O_4$	XRD	Akaogi et al. (1999)
$CaAl_2O_4$	10	$CaFe_2O_4$	XRD	Reid and Ringwood (1969)
Mn_3O_4	12	$CaMn_2O_4$	XRD	Ma et al. (2003)
Fe_3O_4	24 (823 K)	$CaMn_2O_4$	XRD	Fei et al. (1999)
Fe_3O_4	30	$CaTi_2O_4$	XRD	Haavik et al. (2000)
$FeCr_2O_4$	meteorite	$CaTi_2O_4$	XRD	Chen et al. (2003)
$MgFe_2O_4$	25 annealing	$CaMn_2O_4$	XRD	Andrault and Casanova (2001)
$CoFe_2O_4$	32.5	$CaFe_2O_4$	XRD+Raman	Wang et al. (2003a)
$MgMn_2O_4$	15.6	$CaMn_2O_4$	XRD	Malavasi et al. (2005)
$ZnMn_2O_4$	23	Primitive-tetragonal	XRD	Asbrink et al. (1999)
$ZnMn_2O_4$	19	Primitive-tetragonal	calculation	Choi et al. (2006)
Zn_2TiO_4	23.4	$CaTi_2O_4$	XRD+Raman	Wang et al. (2002)
Fe_2TiO_4	11	$CaTi_2O_4$	XRD	Yamanaka et al. (unpublished)
Fe_2TiO_4	45	New phase	XRD	Yamanaka et al. (unpublished)

5. $CaMn_2O_4$ (*Pmab*) transforms to the $CaTi_2O_4$ (*Bbmm*) structure type at about 30 GPa. The latter phase remains unchanged up to 75 GPa. The initial powder pattern was recovered after pressure release, thus the high-pressure phase is unquenchable. Previous Raman and X-ray powder diffraction studies (Wang et al. 2003b) showed that $CaMn_2O_4$ transformed to the $CaTi_2O_4$ structure type at 35 GPa. The reflections of type *hkl*: $h + l = 2n + 1$ found at lower pressures (011, 320, 021, 211, and 221) disappear in the higher-pressure region, because the former has a primitive lattice and the latter a *B*-centered lattice. Hysteresis was not observed upon reducing pressure. The unit-cell volume presented in Table 2 is slightly changed at about 30 GPa as shown in Figure 4. Thus the transition is a first-order transition by atomic displacement from *Pmab* to *Bbmm*, the latter being a minimal non-isomorphic supergroup of the former.

A possible electron spin transition of Mn^{3+} in the octahedral site at transition pressure has been examined. In that case, the high-spin state configuration may change to the low-spin state. The site symmetry of the MnO_6 octahedron is enhanced from 1 in space group *Pmab* to *..m* in *Bbmm* and then the octahedron becomes higher-symmetric with almost equivalent bonds.

A high-low spin transition was proposed for $ZnMn_2O_4$ at 23 GPa by a powder diffraction study (Asbrink et al. 1999) and by a band structure calculation (Choi et al. 2006). Our recent X-ray emission experiments up to 100 GPa do not indicate any change in electronic state or spin configuration up to 50 GPa. The detailed discussion will be published elsewhere.

Interatomic distances calculated from the converged structure parameters show that the Jahn-Teller (JT) distortion caused by Mn^{3+} ($3d^4$) at the octahedral site is evidently observed in lower-pressure $CaMn_2O_4$. The two apical bonds are much longer than the four equatorial bonds. In contrast, after the transformation to the $CaTi_2O_4$-type structure, the six bonds are almost equivalent, as seen from Figure 6.

The suppression of the apical bonds makes the *b* axial length (in *Bbmm* setting) shorten, as shown in Figure 3. We note that the axes (*a b c*) in *Pmab* are changed to (*b a c*) at the transition to the *Bbmm* structure for structural consistency, as seen in Figure 2.

TABLE 2. Lattice parameters of $CaMn_2O_4$, $CaFe_2O_4$, and $CaTi_2O_4$ at high pressures

	P (GPa)	*a* (Å)	*b* (Å)	*c* (Å)	*V* (Å^3)	R_I	R_F	R_p	R_{wp}	S
$CaMn_2O_4$	0.0001	9.6769(1)	9.9880(2)	3.1546(2)	304.90(5)	3.72	1.67	4.74	8.40	2.035
LP phase	0.8	9.619(1)	9.883(2)	3.1076(5)	295.46(7)	9.13	8.99	0.93	1.35	1.045
Pmab	6.0	9.588(2)	9.839(2)	3.0907(6)	291.5(1)	4.71	2.35	2.13	4.71	0.870
	11.1	9.546(2)	9.759(2)	3.0636(7)	285.4(1)	3.28	1.71	1.25	1.77	0.768
	20.4	9.524(2)	9.678(3)	3.0156(7)	277.9(1)	3.09	1.45	0.53	1.61	1.67
	22.7	9.499(1)	9.650(3)	3.001(2)	275.1(1)	3.28	7.26	4.35	1.77	1.915
	24.6	9.457(2)	9.612(3)	2.991(1)	272.4(1)	4.76	2.18	0.53	1.47	1.625
HP phase	31.1	9.451(3)	9.357(2)	2.952(1)	261.2(2)	0.93	0.61	0.85	1.12	0.715
Bbmm	32.3	9.441(3)	9.317(2)	2.9538(7)	259.8(1)	2.14	0.94	0.48	0.73	0.528
	40.5	9.371(2)	9.265(2)	2.9283(6)	254.2(2)	4.54	2.66	0.49	0.71	0.514
	44.7	9.306(1)	9.216(9)	2.913(4)	251.1(5)	6.81	4.17	2.08	4.89	1.235
	49.8	9.264(4)	9.198(3)	2.903(1)	247.3(1)	9.00	5.66	0.71	0.98	0.703
	54.9	9.199(4)	9.178(1)	2.890(1)	244.0(3)	3.85	2.44	0.57	0.81	0.578
	62.0	9.182(4)	9.146(3)	2.877(1)	241.6(1)	6.23	3.69	0.95	1.25	0.676
	75.0	9.148(6)	9.095(4)	2.858(1)	237.8(2)	4.07	2.11	1.04	1.50	0.778
$CaFe_2O_4$	0.0001	9.2239(7)	10.695(1)	3.0191(2)	297.83(3)	1.16	0.67	1.34	1.73	0.435
LP phase	0.1	9.1760(7)	10.647(1)	3.0097(1)	294.04(3)	4.22	2.76	1.24	1.87	1.823
Pnam	8.7	9.1128(9)	10.593(1)	2.9894(2)	288.59(5)	2.26	1.36	1.06	1.51	1.485
	12.6	9.059(1)	10.553(1)	2.9723(4)	284.19(8)	3.21	1.80	1.32	1.88	0.999
	15.5	9.000(1)	10.503(1)	2.9555(4)	279.39(8)	1.92	0.92	1.06	1.51	1.067
	18.9	8.946(2)	10.465(2)	2.9404(7)	275.3(1)	3.06	1.33	1.27	1.84	1.467
	22.7	8.886(2)	10.406(2)	2.9271(7)	270.6(1)	2.19	1.05	1.22	1.68	0.917
	29.5	8.830(2)	10.336(2)	2.9159(7)	266.1(1)	1.89	1.30	0.96	1.29	1.021
	35.5	8.777(2)	10.292(2)	2.9033(4)	262.30(9)	2.22	1.15	1.31	1.79	1.331
	42.6	8.718(1)	10.239(2)	2.8890(3)	257.89(7)	3.33	1.46	1.00	1.41	1.184
	44.7	8.676(1)	10.207(2)	2.8778(4)	254.87(8)	1.34	0.75	1.15	1.43	1.344
New HP phase	51.4	8. 493(9)	9.658(5)	8. 438(5)	692.8(2)	3.58	1.84	1.80	1.34	1.258
Pnam	63.3	8.376(5)	9.551(5)	8.353(1)	668.2(2)	1.26	0.61	1.87	1.48	1.178
$CaTi_2O_4$	0.0001	9.7390(9)	9.9738(8)	3.1518(3)	306.15(5)	5.58	3.58	4.74	6.71	0.772
LP phase	3.0	9.6898(7)	9.9495(5)	3.1418(3)	302.90(3)	5.39	3.03	1.17	1.87	1.277
Bbmm	7.7	9.6121(9)	9.8929(7)	3.1245(2)	297.12(4)	3.41	2.23	1.24	1.92	1.849
	13.6	9.523(1)	9.840(1)	3.1021(5)	290.73(8)	1.62	0.99	1.24	1.80	1.621
	18.6	9.466(3)	9.805(2)	3.0865(8)	286.5(1)	3.53	1.92	1.36	1.90	2.449
	25.3	9.394(4)	9.750(2)	3.058(1)	280.1(1)	1.68	0.86	1.15	1.65	1.446
	29.8	9.338(6)	9.718(4)	3.026(1)	274.7(3)	3.25	1.50	1.29	1.86	1.892
New HP phase	39.8	9.257(5)	9.642(3)	8.967(2)	800.4(2)	7.50	3.90	1.26	1.62	1.751
Bbmm	45.5	9.238(5)	9.597(4)	8.886(1)	787.5(2)	5.67	3.05	1.22	1.57	2.268
	75.0	9.104(6)	9.403(3)	8.635(5)	739.1(7)	9.52	4.61	1.10	1.53	3.526
	80	9.086(8)	9.335(4)	8.585(7)	729.7(1.0)	8.96	4/11	0.98	1.47	2.771

Notes: The reliability factors are

$$R_p = \frac{\sum_i |y_i - f_i(x)|}{\sum_i y_i}, \quad R_{wp} = \left[\frac{\sum_i w_i \{y_i - f_i(x)\}^2}{\sum_i w_i y_i^2} \right]^{\frac{1}{2}}, \text{ and } S = \left[\frac{\sum_i w_i \{y_i - f_i(x)\}^2}{N - P} \right]^{\frac{1}{2}},$$

where y_i is the observed intensity at *i* position in 2θ. $f_i(x)$ is the calculated intensity. w_i is a weight. *N* and *P* indicate the total number of the data points and variable parameters, respectively. I and F indicate integrated intensity and structure factor, respectively.

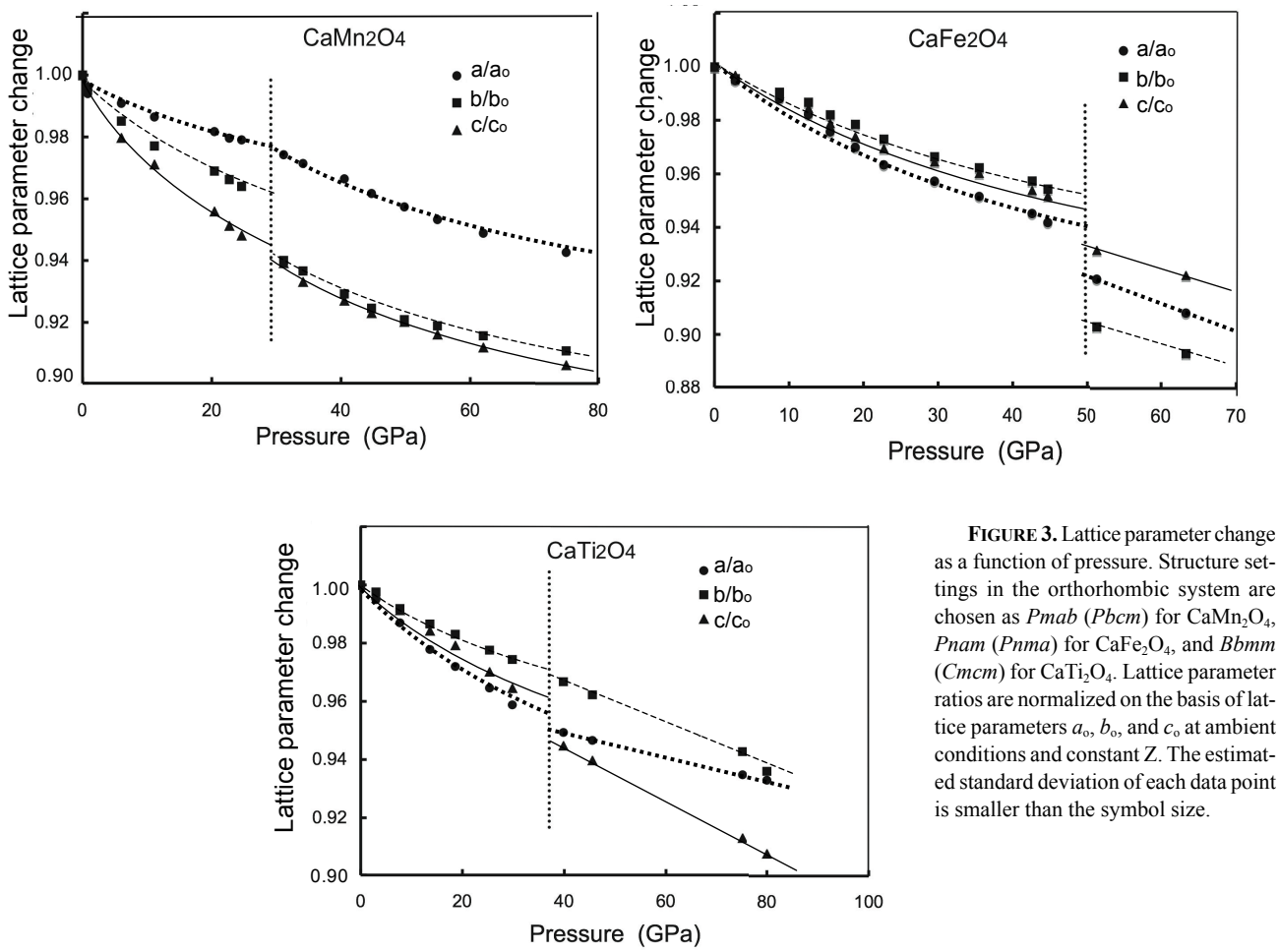

FIGURE 3. Lattice parameter change as a function of pressure. Structure settings in the orthorhombic system are chosen as *Pmab* (*Pbcm*) for $CaMn_2O_4$, *Pnam* (*Pnma*) for $CaFe_2O_4$, and *Bbmm* (*Cmcm*) for $CaTi_2O_4$. Lattice parameter ratios are normalized on the basis of lattice parameters a_o, b_o, and c_o at ambient conditions and constant Z. The estimated standard deviation of each data point is smaller than the symbol size.

Pressure	Space group	*a* (Å)	*b* (Å)	*c* (Å)	Volume
Before transition:					
24.6 GPa	*Pmab*	9.457(2)	9.612(3)	2.991(1)	272.4(1)
After transition:					
31.1 GPa	*Bbmm*	9.451(3)	9.357(2)	2.952(1)	262.1(2)

The unit-cell volume is reduced by 3.8% after the transition. The JT-distortion in the MnO_6 octahedron disappears in the high-pressure phase. The lower-pressure phase of $CaMn_2O_4$ has an axial relation of $b > a > c$. On the other hand, the lattice parameters in the higher-pressure phase of the $CaTi_2O_4$-type structure are $a > b > c$ and the crystallographic *a*-direction in *Bbmm* is equivalent to the *b*-direction in *Pmab*. However, the $CaTi_2O_4$ (also *Bbmm*) structure has $b > a >$ c as can be seen in Table 2 and below.

High-pressure diffraction study of $CaFe_2O_4$

All atoms of $CaFe_2O_4$ (*Pnam*) are in Wyckoff positions 4*c*: ± (x, y, 1/4; x + 1/2, –y + 1/2, 1/4). The low-pressure form transforms to a new high-pressure phase at 51.4 GPa. The diffraction patterns are presented in Figure 7. The high-pressure phase is unquenchable and shows a reversible transition at 42.8 GPa. Since the diffraction pattern at 63.3 GPa is taken only from the new phase without any residual peaks of the lower-pressure phase, structure analysis of the new phase detected from the pattern was performed first by indexing with DICVOL written by Boultif and Louer (2004), using 12 reflections in 2θ = 4–16°. A most probable index set with the orthorhombic structure was chosen from several candidates. Two possible space groups, i.e., *Pnam* (no. 62) and $Pnm2_1$ (no. 33) among structures with the *P*-lattice were given from the extinction conditions for the *hkl* indices using EXP02004 (Altomare et al. 2005). The former is a centric and the latter a non-centrosymmetric structure. The correct space group cannot be determined by the diffraction method because of the Friedel rule. In the next step a Monte Carlo calculation was applied to find the possible structure models with these space groups. Finally, Rietveld profile fitting was carried out using the program RIETAN written by Izumi and Ikeda (2000). The fitting calculation considered the atomic positional parameters, FWHM parameters, asymmetry parameters of the profile, and background parameters. However, site occupancy parameters were not varied, because the ionic radii of Ca and Fe^{2+} are too different for intracrystalline exchange in two sites. The most reliable fitting was provided after several trials based on various initial models proposed by the Monte Carlo method. The final data set with $R_p = 1.48$, $R_{wp} = 1.87$, $R_I = 1.26$, $R_F = 0.61$, and S = 1.178 is presented in Table 3 and the fitting pattern is shown in Figure 8. The Rietveld analysis provided the structure of the new phase with space group *Pnam*, $Z = 12$, and lattice parameters $a = 8.376(5)$ Å, $b = 9.551(5)$ Å, $c = 8.353(1)$ Å, $V = 668.2(2)$ Å^3, and density = 6.43 g/cm^3 at 63.3 GPa. The density is increased by 9.4% in the new phase.

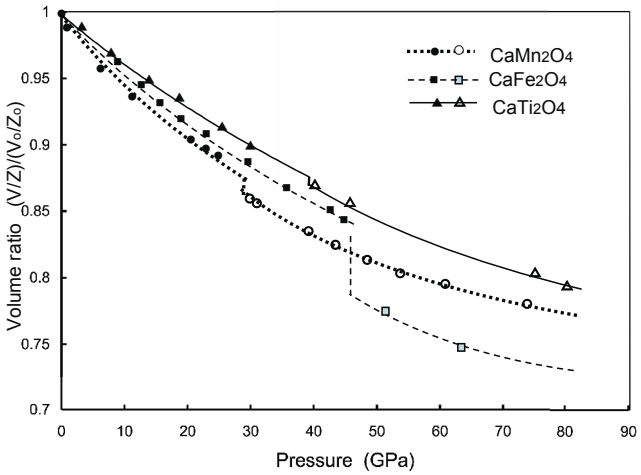

FIGURE 4. Pressure dependence of the unit-cell volume. The vertical axis indicates $(V/Z)/(V_o/Z_o)$ to have consistency in the volume change, because of changes in Z between low- and high-pressure phases. The estimated standard deviation of each data point is smaller than the symbol size.

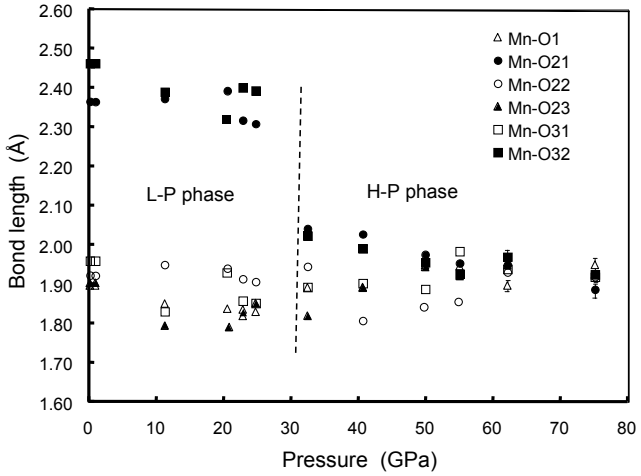

FIGURE 6. Mn-O bond distances of the MnO_6 octahedron in $CaMn_2O_4$ vs. pressure. Jahn-Teller distortion in the octahedral site disappears at pressures above 30 GPa. The error bars are smaller than the symbol size except those at high pressures (62 and 75.0 GPa).

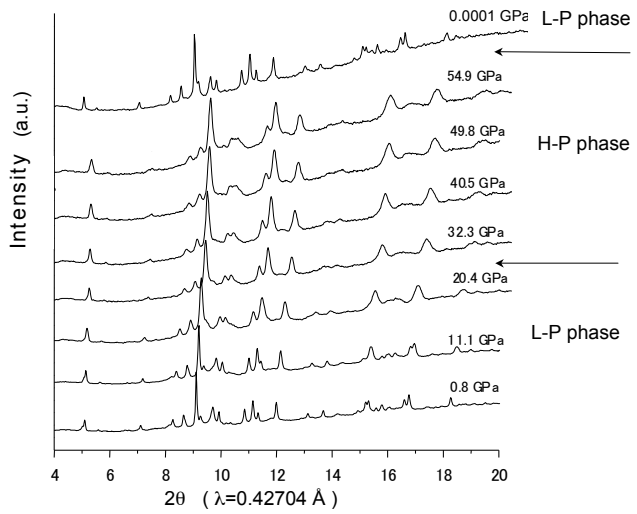

FIGURE 5. Powder diffraction patterns of $CaMn_2O_4$ under high pressures.

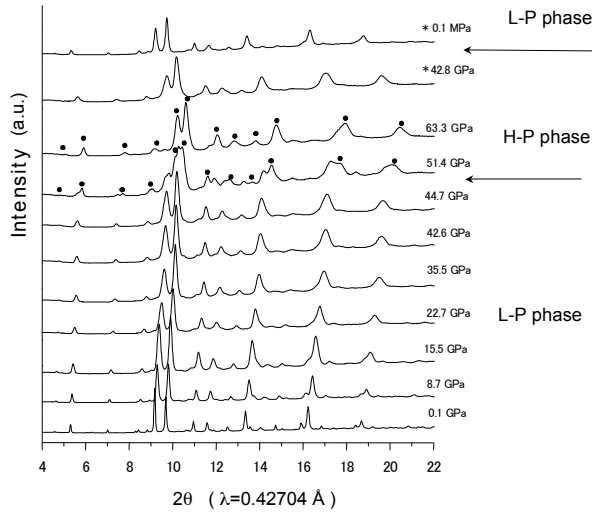

FIGURE 7. Powder diffraction patterns of $CaFe_2O_4$ under high pressures. Peaks marked by solid circles are from the new high-pressure phase. The diffraction patterns marked with * were observed after releasing pressure.

The *c*-axis dimension of the new high-pressure structure is about three times larger than that of the low-pressure structure of $CaFe_2O_4$ but both structures have the same space group symmetry *Pnam*. The symmetry of the former belongs to the maximal isomorphic subgroup of the latter. Since the octahedral layer is compressed, the repulsion between adjacent Fe cation layers induces a shift of the layer in the direction parallel to [100]. All axes become shortened at the transition. The *b* axial length is the most noticeably reduced, as seen in Figure 4.

The low-pressure (LP) structure of $CaFe_2O_4$ is constructed by two cation layers of Fe and Ca in the same mirror plane. In contrast, the new high-pressure (HP) structure is composed of six cation layers. If three LP structures are piled along the *c* axis and every third cation layer is shifted parallel to the *a* axis due to the compression of [001], it produces the HP structure. Figure 9 is a schematic drawing of the shift in every third layer. The martensitic transition is generated by the new atomic arrangement of the HP structure. All Fe atoms in the LP structure occupy the 4*c* position on the mirror plane. However, in the HP phase only four Fe atoms are located at 4*c* positions, while the other eights are on general 8*d* positions. The two non-identical Ca atoms are on 4*c* and 8*d* positions.

High-pressure diffraction study of $CaTi_2O_4$

$CaTi_2O_4$ with space group *Bbmm* (*Cmcm*) contains trivalent titanium Ti^{3+} ($3d^1$) and is grown under conditions of low oxidation potential. Powder diffraction studies have been carried out with increasing pressure up to 80 GPa. The diffraction patterns

TABLE 3. Rietveld analysis of the new HP phase of $CaFe_2O_4$ (*Pnam*) at 63.3 GPa

Atom	Wyck.	Site sym.	x	y	z
Ca1	4*c*	..*m*	0.780(8)	0.332(10)	1/4
Fe1	4*c*	..*m*	0.397(6)	0.390(8)	1/4
Fe2	4*c*	..*m*	0.403(11)	0.898(10)	1/4
O1	4*c*	..*m*	0.208(7)	0.838(7)	1/4
O2	4*c*	..*m*	0.136(2)	0.534(2)	1/4
O3	4*c*	..*m*	0.494(6)	0.227(8)	1/4
O4	4*c*	..*m*	0.410(2)	0.574(3)	1/4
Ca2	8*d*	1	0.715(6)	0.851(5)	0.085(5)
Fe3	8*d*	1	0.567(4)	0.614(5)	0.087(11)
Fe4	8*d*	1	0.087(5)	0.395(5)	0.082(8)
O5	8*d*	1	0.787(15)	0.160(15)	0.073(13)
O6	8*d*	1	0.885(10)	0.477(12)	0.083(8)
O7	8*d*	1	0.485(14)	0.779(9)	0.090(6)
O8	8*d*	1	0.085(8)	0.078(6)	0.116(10)

Note: Reliability factors are R_p = 1.48, R_{wp} = 1.87, R_I = 1.26, R_F = 0.61, and S = 1.178.

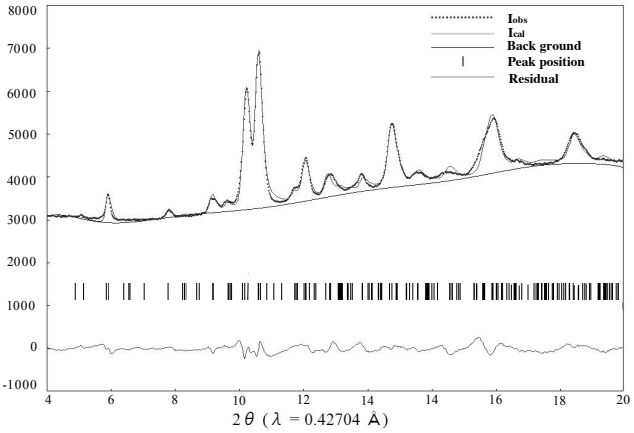

FIGURE 8. Rietveld profile fitting of the new high-pressure phase of $CaFe_2O_4$. The diffraction pattern was taken at 63.3 GPa.

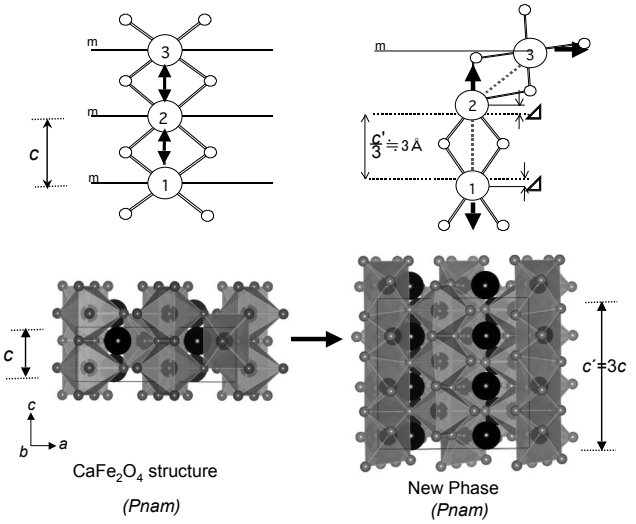

FIGURE 9. Atomic arrangement in $CaFe_2O_4$ viewed parallel to the *b* axis. Left: low-pressure phase, right: new high-pressure phase at 63.3 GPa. Every third layer of the low-pressure structure shifts by martensitic transformation in the direction of the *a* axis and thus produces the high-pressure structure. The interlayer distance parallel to the *c* axis is changed by the transition. In the lower figures, the large spheres indicate Ca ions and the small ones oxygen atoms. Iron is hidden in polyhedra.

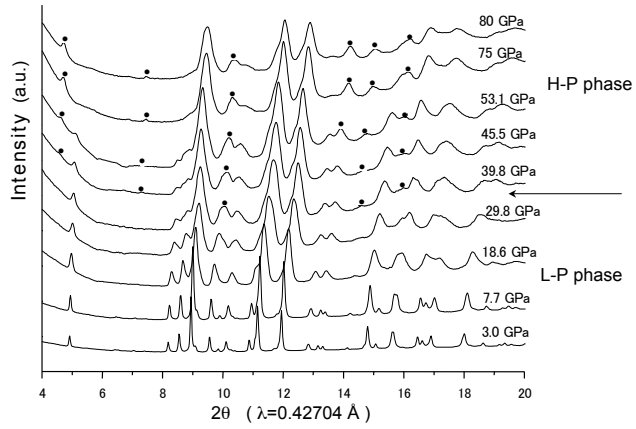

FIGURE 10. Powder diffraction patterns of $CaTi_2O_4$ with increasing pressure. Peaks marked with solid circles are distinguishing peaks of the new phase.

are shown in Figure 10. The structure is very similar to $CaMn_2O_4$ (*Pmab*) as presented in Figure 2, but differs in that all atoms of the former are located on the mirror plane perpendicular to the *c* axis. These two structures are crystallographically closely related via the maximal/minimal isomorphic sub- and supergroups. New peaks were observed after transformation to another high-pressure phase at 39.6 GPa. The back-transformation was confirmed at 31.6 GPa. Consequently it has been proven (1) that the phase is not decomposed but transformed; (2) that the high-pressure phase is unquenchable; and (3) that there is a considerable pressure range of hysteresis. The new phase is stable at pressures up to the maximum experimental pressure of 80 GPa. The diffraction pattern is not similar to the new phase found in $CaFe_2O_4$ shown in Figure 8.

The indexing of the 12 reflections at 2θ = 4–19° of the powder pattern taken at 80 GPa has been performed with DICVOL. Possible space groups were determined from the extinction conditions found in the indices. The following three space groups were candidates for the new phase: *Bbmm* (*Cmcm*), *Bbm*2 (*C*2*cm*), or $Bb2_1m$ ($Cmc2_1$). Using the diffraction pattern observed at 80 GPa, several possible structure candidates for each space group were provided by the Monte Carlo method. Finally, Rietveld profile fitting was applied for these candidates. The density changes about 6% at the transition pressure.

The Rietveld profile fitting based on space group *Bbmm* provides the most reliable result, which is presented in Table 4. The lattice parameters of the new phase are *a* = 9.086(8) Å, *b* = 9.335(4) Å, *c* = 8.585(7) Å, *V* = 729.7(1.0) Å^3, *Z* = 12, and density = 5.45 g/cm^3. The *c* axis of the new structure is about three times larger than that of the low-pressure structure of $CaTi_2O_4$. The transition mechanism is very similar to the afore-mentioned transition found in $CaFe_2O_4$, but the transition is simply a martensitic transformation with rearrangement of atoms in the layer. The high-pressure structure has the same space group, *Bbmm*, as the low-pressure phase and the former symmetry belongs to the maximal isomorphic subgroup of the latter.

DISCUSSION

Bulk modulus of the three post-spinel phases

The unit-cell volume changes vs. pressure of the three post-spinel phases are illustrated in Figure 4. The bulk moduli are calculated by the Birch-Murnaghan equation of state using the observed volumes as a function of pressure (Table 2). The calculation provides K_0 = 155(2) GPa for $CaMn_2O_4$, 196(2) GPa for $CaFe_2O_4$, and 224(7) GPa for $CaTi_2O_4$ in the lower-pressure phases. In the calculation K_0' is fixed to 4.0. The $CaMn_2O_4$ high-pressure phase of the $CaTi_2O_4$-type structure has K_0 = 193(3) GPa. Among the three structures, $CaTi_2O_4$ has the largest bulk modulus. The new phase of $CaTi_2O_4$ that occurs at higher pressure has a different structure from the high-pressure phase of $CaFe_2O_4$. The reliable bulk moduli of both new HP phase of $CaFe_2O_4$ and $CaTi_2O_4$ could not be obtained, because of only a small number of the observed data.

The relatively stable regions of these three post-spinel type structures under high pressure are related to the octahedral trivalent cations. Based simply on the rigid ("hard-sphere") ion model, $CaTi_2O_4$ is composed of the largest octahedral cation among the three post-spinels and would be more compressible than the other two stoichiometries according to the ionic radii: Mn^{3+} (0.645 Å), Fe^{3+} (0.645 Å), and Ti^{3+} (0.670 Å) (Shannon 1976). Yet the structure has the largest bulk modulus.

The three post-spinel structures have a similar herringbone structure about the Ca atom in the edge-sharing plane perpendicular to the *c* axis, as shown in Figure 2. However, the arrangement of M_2O_{10} (M = Mn, Fe, Ti) dimers of MO_6 octahedra in these structures is different. MnO_6 and TiO_6 octahedra are very similar but different from the FeO_6 octahedra. The structures of $CaMn_2O_4$ and $CaTi_2O_4$ are similar in this respect, i.e., the M_2O_{10} octahedral dimers are linked via common edges. On the other hand in $CaFe_2O_4$, the octahedral dimers are linked via corner sharing. These different linkages affect the compressibilities significantly. From the freedom of displacement of each atom, the structure of $CaMn_2O_4$ is the most flexible and thus compressible, because there are more variable positional parameters than in those of the two others. In contrast, all atoms of $CaFe_2O_4$ and $CaTi_2O_4$ are located on the mirror planes and therefore are tightly constrained in their atomic displacement. Consequently the site symmetries and octahedral linkages also control the compressibilities of the three samples.

The electronic state of the transition elements also results in a large effect on the compressibility. Spinels composed of JT elements with $3d^{4+}$ electronic configuration in the B site (octahedral site) may transform to the $CaMn_2O_4$-type structure as their post-spinel phase, such as Mn_3O_4 (Ma et al. 2003) and $MgMn_2O_4$ (Malavasi et al. 2005), because the $CaMn_2O_4$-type structure is characteristic of JT distorted octahedra.

TABLE 4. Rietveld analysis of the new high-pressure phase of $CaTi_2O_4$ (*Bbmm*) at 80 GPa

Atom	Wyck.	Site sym.	x	y	z
Ca1	4*c*	2*mm*	0.381(6)	1/4	0.0
Ca2	8*g*	*.m.*	0.118(9)	3/4	0.166(7)
Ti1	8*f*	*..m*	0.127(10)	0.064(8)	0.0
Ti2	16*h*	1	0.372(9)	0.935(8)	0.1667
O11	4*b*	..2/*m*	1/2	0.0	0.0
O12	8*e*	..2	0.0	0.0	0.1667
O21	4*c*	2*mm*	0.059(13)	1/4	0.0
O22	8*g*	*.m.*	0.440(7)	3/4	0.166(7)
O31	8*f*	*..m*	0.230(13)	–0.106(1)	0.0
O32	16*h*	1	0.269(7)	0.393(9)	0.1667

Note: Reliability factors are R_P = 0.98, R_{WP} = 1.47, R_I = 8.96, R_F = 4.111, and S = 2.771.

Further consideration on high-pressure phase transformations of spinels

$MgAl_2O_4$ spinel is one of the minerals present in the crust of the Earth and has received much attention from the viewpoint of being a potential aluminum reservoir in the Earth's mantle and subduction zones. $MgAl_2O_4$ first decomposes to MgO and Al_2O_3 at 15 GPa (Akaogi et al. 1999) and these are crystallized as the $CaFe_2O_4$-type structure at 25–28 GPa (Akaogi et al. 1999; Irifune et al. 1991, 1998). Hence the $CaFe_2O_4$ phase is the most probable Al reservoir phase in the mantle or subduction zones. Yet later, the $CaTi_2O_4$-type structure was predicted as the highest-pressure polymorph of $MgAl_2O_4$ by ab initio calculation (Catti 2001). It has since been shown by XRD that the spinel actually changes to the $CaTi_2O_4$-type structure (Funamori et al. 1998), and the structure is confirmed to be stable up to 117 GPa (Ono et al. 2006). In contrast, the present experiments demonstrate that $CaFe_2O_4$ does not transform to the $CaTi_2O_4$-type structure but to a new structure.

The $CaMn_2O_4$-, $CaTi_2O_4$-, and $CaFe_2O_4$-type structures are major candidates for post-spinel phases in the Earth's mantle. The $CaMn_2O_4$-type structure appears only reasonable as a high-pressure phase of spinels bearing JT cations. As shown in the schematic diagram in Figure 11, these spinels first transform to the $CaMn_2O_4$ post-spinel type structure and then further transform to the $CaTi_2O_4$ type under higher pressure. The present experiment found a new high-pressure phase of $CaTi_2O_4$. Among the three post-spinel candidates $CaTi_2O_4$ has the largest bulk modulus.

The present experiments have been conducted under high-pressure conditions at ambient temperature. A consideration on the influence of temperature in general would provide the possibility of other phases. The solid solution $(Mg_xCa_{1-x})Al_2O_4$ (x = 0.66–0.8) transforms to a hexagonal structure above 1200 °C and 15 GPa (Akaogi et al. 1999) and the structure was determined by Miura et al. (2000). Recently we found a new phase of $CaMn_2O_4$

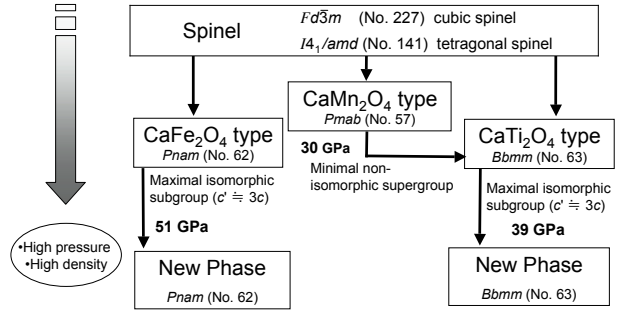

FIGURE 11. Diagram of the phase relations of post-spinels. Arrows indicate the direction of pressure increase. The space-group symmetry relations are presented with increasing pressure. The high-pressure phase transitions are reversible.

at 95 GPa after laser heating. Probably some other polymorphs of post-spinel phases or further high-pressure transformations will be found under combined high pressure and temperature.

ACKNOWLEDGMENTS

We give grateful thanks to Wilson Crichton in ESRF for his useful discussion and comments for the publication. The present investigation was performed under the auspice of KEK proposals no. 2002G199 for powder diffraction study at BL-13A and 18C.

REFERENCES CITED

Akaogi, M., Hamada, Y., Suzuki, T., Kobayashi, M., and Okada, M. (1999) High-pressure transitions in the system $MgAl_2O_4$-$CaAl_2O_4$: A new aluminous phase with implication for the lower mantle. Physics of the Earth and Planetary Interiors, 115, 67–77.

Altomare, A., Camalli, M., Cuocci, C., da Silva, C., Giacovazzo, C., Moriterni, A.G.G., and Rizza, R. (2005) Space group determination: improvements in EXPO2004. Journal of Applied Crystallography, 38, 760–767.

Andrault, D. and Casanova, N.B. (2001) High-pressure phase transitions in the $MgFe_2O_4$ and Fe_2O_3-$MgSiO_3$ systems. Physics and Chemistry of Minerals, 28, 211–217.

Asbrink, S., Wakkowska, A., Gerward, L., Olsen, J.S., and Talik, E. (1999) High-pressure phase transition and properties of spinel $ZnMn_2O_4$. Physical Review B, 60, 12651–12656.

Boultif, A. and Louer, D. (2004) Powder pattern indexing with the dichotomy method. Journal of Applied Crystallography, 37, 724–731.

Burnley, P.C., Green, H.W., and Prior, D. (1991) Faulting associated with the olivine to spinel transformation in Mg_2GeO_4 and its implications for deep-focus earthquakes. Journal of Geophysical Research, 96, 425–443.

Chen, M., Shu, J., Xie, X., and Mao, H.K. (2003) Natural $CaTi_2O_4$-structured $FeCr_2O_4$ polymorph in the Suizhou meteorite and its significance in mantle mineralogy. Geochimica et Cosmochimica Acta, 67, 3937–3942.

Catti, M. (2001) High-pressure stability, structure and compressibility of *Cmcm*-$MgAl_2O_4$: an ab initio study. Physics and Chemistry of Minerals, 28, 729–736.

Choi, H.C., Shim, J.H., and Min, B. (2006) Electronic structures and magnetic properties of spinel $ZnMn_2O_4$ under high pressure. Physical Review B, 74, 172103.

Decker, B.F. and Kasper, J.S. (1957) The structure of calcium ferrite. Acta Crystallographica, 10, 332–337.

Fei, Y., Mao, H.K., Hemley, R.J., Shu, J., and Shen, G. (1999) In situ structure determination of the high-pressure phase of Fe_3O_4. American Mineralogist, 84, 203–206.

Funamori, N., Jeanloz, R., Nguyen, H., Kavner, A., and Caldwell, W.A. (1998) High-pressure transformation in $MgAl_2O_4$. Journal of Geophysical Research, 103, 20813–20818.

Geisber, H.G., Pennington, W.T., and Kolis, J.W. (2001) Redetermination of $CaMn_2O_4$. Acta Crystallographica C, 57, 329–330.

Haavik, C., Tolen, S., Fjellvag, H., Hanfland, M., and Hauserman, D. (2000) Equation of state of magnetite and its high-pressure modification: Thermodynamics of Fe-O system at high pressure. American Mineralogist, 85, 514–523.

Hahn, T.D. (1983) International Tables for Crystallography, volume A: Space Group Symmetry. Reidel Publishing Company, Dordrecht.

Harrison, R.J., Dove, M.T., Knight, K.S., and Putnis, A. (1999) In situ neutron diffraction study of non-convergent cation ordering in the $(Fe_3O_4)_{1-x}(MgAl_2O_4)_x$ spinel solid solution. American Mineralogist, 84, 555–563.

Hill, R.J., Craig, J.R., and Gibbs, G.V. (1979) Systematics of the spinel structure types. Physics and Chemistry of Minerals, 4, 317–339.

Irifune, T., Fujino, K., and Ohtani, K. (1991) A new high-pressure form of $MgAl_2O_4$. Nature, 349, 409–411.

Irifune, T., Nishiyama, N., Kuroda, K., Inoue, T., Isshiki, M., Utsumi, W., Funakoshi, K., Urakawa, S., Uchida, T., and Katsura, T. (1998) Postspinel phase boundary in Mg_2SiO_4 determined by in situ X-ray diffraction. Science, 279, 1698–1700.

Ito, E. and Takahashi, E. (1989) Postspinel transformations in the system Mg_2SiO_4-Fe_2SiO_4 and some geophysical implications. Journal of Geophysical Research, 94, 10637–10646.

Izumi, F. and Ikeda, T. (2000) A Rietveld-analysis program RIETAN-98 and its applications to zeolites. European Powder Diffraction, Materials Science Forum, 198–203.

Kiefer, B., Stixrude, L., and Wentzcovitch, R.M. (1997) Calculated elastic properties and anisotropy of Mg_2SiO_4 spinel at high pressure. Geophysical Research Letter, 24, 2841–2844.

Kirby, S.H., Stein, S., Okai, E.A., and Rubie, D.C. (1996) Metastable mantle phase transformations and deep earthquakes in subducting oceanic lithosphere. Review of Geophysics, 34, 261–306.

Lavina, B., Salviulo, G., and Giusta, A.D. (2002) Cation distribution and structure modeling of spinel solid solutions. Physics and Chemistry of Minerals, 29, 10–18.

Leven, J.H., Jackson, I., and Ringwood, A.E. (1981) Upper mantle seismic anisotropy and lithospheric decoupling. Nature, 289, 234–239

Li, L., Cares, P., and Weidner, D.J. (2007) Effect of cation ordering and pressure on spinel elasticity by ab initio simulation. American Mineralogist, 92, 174–178.

Ma, Y., Yang, H., and Prewitt, C.J. (2003) High-pressure X-ray diffraction studies of Mn_3O_4 to 40 GPa. American Physical Society Annual Meeting, p. 3–7.

Malavasi, L., Tealdi, C., Amboage, M., Mozzatti, M.C., and Flor, G. (2005) High-pressure X-ray diffraction study of $MgMn_2O_4$ tetragonal spinel. Nuclear Instruments and Methods in Physics Research B, 238, 171–174.

Mao, H.K., Xu, J., and Bell, P.M. (1986) Calibration of the ruby pressure gauge to 800 kbar under quasi-hydrostatic conditions. Journal of Geophysical Research, 91, 4673–4676.

Méducin, F., Redfern, S.A.T., Godec, Y.L., Stone, H.J., Trucker, M.G., Dove, M.T., and Marshall, W.G. (2004) Study of cation order-disorder in $MgAl_2O_4$ spinel by in situ neutron diffraction up to 1600 K and 3.2 GPa. American Mineralogist, 89, 981–986.

Meng, Y., Weidner, D.J., Gwanmesia, G. D., Lieberman, R.C., Vaughan, M.T., Wang, Y., Leinenweber, K., Pacalo, R.E., Yeganeh-Haeri, A., and Zhao, Y. (1993) In situ high *P-T* X-ray diffraction studies on three polymorphs (α,β,γ) of Mg_2SiO_4. Journal of Geophysical Research, 98, 22199–22207.

Miura, H., Hamada, Y., Suzuki, T., Akaogi, M., Miyajima, N., and Fujino, K. (2000) Crystal structure of $CaMg_2Al_6O_{12}$, a new Al-rich high pressure form. American Mineralogist, 85, 1799–1803.

Morishima, H., Kato, T., Suto, M., Ohtani, E., Urakawa, S., Utsumi, W., Shimomura, O., and Kikegawa, T. (1994) The phase boundary between α- and β-Mg_2SiO_4 determined by in situ X-ray observation. Science, 265, 1202–1203.

Ohtaka, O., Tobe, H., and Yamanaka, T. (1997) Phase equilibria for the Fe_2SiO_4-Fe_3O_4 system under high pressure. Physics and Chemistry of Minerals, 24, 555–560.

Ono, S., Kikegawa, T., and Ohishi, Y. (2006) The stability and compressibility of $MgAl_2O_4$ high-pressure polymorphs. Physics and Chemistry of Minerals, 33, 200–206.

Pavese, A., Artioli, G., and Hull, S. (1999) In situ neutron powder diffraction of cation portioning vs. pressure in $Mg_{0.94}Al_{2.04}O_4$ synthetic spinel. American Mineralogist, 84, 905–912.

Peterson, R.C., Lager, G.A., and Hitterman, R.L. (1991) A time-of-flight powder diffraction study of $MgAl_2O_4$ at temperatures up to 1273 K. American Mineralogist, 76, 1455–1458.

Piermarini, G.J., Blook, S., Barnett, J.D., and Forman, R.A. (1975) Calibration of the pressure dependence of the R1 ruby fluorescence line to 195 kbar. Journal of Applied Physics, 46, 2774–2780.

Reid, A.F. and Ringwood, A.E. (1969) Newly observed high-pressure transformations in Mn_3O_4, $CaAl_2O_4$, and $ZrSiO_4$. Earth and Planetary Science Letter, 6, 205–208.

Rogge, M.P., Caldwell, J.H., Ingram, D.R., Green, C.E., Geselbracht, M.J., and Siegrist, T. (1998) A new synthetic route to peseudo-brookite-type $CaTi_2O_4$. Journal of Solid State Chemistry, 141, 338–342.

Sawamoto, H., Weidner, D., Sasaki, S., and Kumazawa, M. (1984) Single-crystal elastic properties of the modified spinel (beta) phase of magnesium orthosilicate. Science, 224, 749–751.

Schwandt, C. and Fray, D.J. (2005) Determination of kinetic pathway in the electrochemical reduction of titanium dioxide in molten calcium chloride. Electrochemica Acta, 51, 66–76.

Shannon, R.D. (1976) Revised effective ionic radii and systematics of interatomic distances in halides and chalcogenides. Acta Crystallographica A, 32, 751–767.

Shim, S.H., Duffy, T.S., and Shen, G. (2001) The post-spinel transformation in Mg_2SiO_4 and its relation to the 660 km seismic discontinuity. Nature, 411, 571–574.

Wang, Z., Saxena, S.K., and Zha, C.S. (2002) In situ X-ray diffraction and Raman spectroscopy of pressure-induced phase transformation in spinel Zn_2TiO_4. Physical Review B, 66, 024103.

Wang, Z., Downs, R.T, Pischedda, V., Shetty, R., Saxena, S.K., Zha, C.H., Zhao, Y.S., Schiferi, D., and Waskowska, A. (2003a) High-pressure X-ray diffraction and Raman spectroscopy studies of the tetragonal spinel $CoFe_2O_4$. Physical Review B, 68, 94101–94107.

Wang, Z., Saxena, S.K., and Neumeier, J.J. (2003b) Raman scatting study on pressure-induced phase transformation of marokite ($CaMn_2O_4$). Journal of Solid State Chemistry, 170, 382–389.

Xu, Y., Poe, B.T., Shankland, T.J., and Rubie, D.C. (1998) Electrical conductivity of olivine, wadsleyite and ringwoodite under upper-mantle conditions. Science, 280, 1415–1418.

Yamanaka, T. and Okita, M. (2001) Magnetic Properties of the Fe_2SiO_4-Fe_3O_4 spinel solid solution. Physics and Chemistry of Minerals, 28, 102–109.

Yamanaka, T. and Takeuchi, Y. (1983) Order-disorder transition in $MgAl_2O_4$ spinel at high temperatures up to 1700 °C. Zeitschrift für Kristallographie, 165, 65–78.

Yamanaka, T., Shimazu, H., and Ota, K. (2001) Electric Conductivity of the Fe_2SiO_4-Fe_3O_4 Spinel Solid Solution. Physics and Chemistry of Minerals, 28, 110–118.

MANUSCRIPT RECEIVED JANUARY 17, 2008
MANUSCRIPT ACCEPTED JUNE 9, 2008
MANUSCRIPT HANDLED BY EUGEN LIBOWITZKY